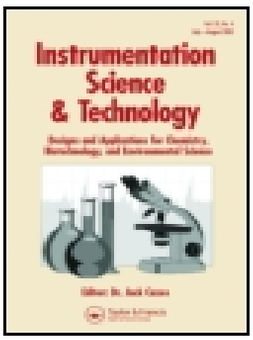

Instrumentation Science & Technology

ISSN: 1073-9149 (Print) 1525-6030 (Online) Journal homepage: http://www.tandfonline.com/loi/list20

Real-time, label-free characterization of oligosaccharide-binding proteins using carbohydrate microarrays and an ellipsometry-based biosensor

Yung-Shin Sun & X. D. Zhu

To cite this article: Yung-Shin Sun & X. D. Zhu (2017): Real-time, label-free characterization of oligosaccharide-binding proteins using carbohydrate microarrays and an ellipsometry-based biosensor, Instrumentation Science & Technology, DOI: 10.1080/10739149.2016.1278017

To link to this article: http://dx.doi.org/10.1080/10739149.2016.1278017

Accepted author version posted online: 03 Jan 2017.
Published online: 03 Jan 2017.

INSTRUMENTATION SCIENCE AND TECHNOLOGY
http://dx.doi.org/10.1080/10739149.2016.1278017

Taylor & Francis
Taylor & Francis Group

Real-time, label-free characterization of oligosaccharide-binding proteins using carbohydrate microarrays and an ellipsometry-based biosensor

Yung-Shin Sun[a] and X. D. Zhu[b]

[a]Department of Physics, Fu Jen Catholic University, New Taipei City, Taiwan; [b]Department of Physics, University of California, Davis, California, USA

ABSTRACT

Carbohydrates present on cell surfaces mediate cell behavior through interactions with other biomolecules. Due to their structural complexity, diversity, and heterogeneity, it is difficult to fully characterize a variety of carbohydrates and their binding partners. As a result, novel technologies for glycomics applications have been developed, including carbohydrate microarrays and label-free detection methods. In this paper, we report using the combination of oligosaccharide microarrays and the label-free oblique-incidence reflectivity difference microscopy for real-time characterization of oligosaccharide-binding proteins. Aminated human milk oligosaccharides were immobilized on epoxy-coated glass substrates as microarrays for reactions with Family 1 of solute-binding proteins from *Bifidobacterium longum* subsp. *infantis* (*B. infantis*). Binding affinities of these protein–oligosaccharide interactions showed preferences of Family 1 of solute-binding proteins to host glycans, which helps in characterizing the complex process of human milk oligosaccharides foraging by *B. infantis*.

KEYWORDS

Carbohydrate microarray; label-free biosensor; oblique-incidence reflectivity difference; real-time kinetics; solute binding proteins

Introduction

Carbohydrates play important roles in a wide range of biochemical interactions because all cells are surrounded by layers mostly composed of oligo- and polysaccharides.[1,2] These sugars act as a part of the protective layers defending cells against harmful physical impact. Moreover, through interactions with other biomolecules, they regulate cell behaviors, especially those involving surfaces such as cell–cell interactions,[3,4] cell adhesion,[5,6] and cell motility.[7,8] Certain protein–carbohydrate interactions are crucial to biological processes such as metastasis,[9] immune response,[10,11] and pathogen-host infections.[12] Considering the infectious virus as an example, the virus uses surface glycoprotein hemagglutinin to attach itself to a host cell surface and initiate transfer of viral genome into infected cell through binding to sialosides on the surface of the cell.[13,14] Abnormal expression of

CONTACT Yung-Shin Sun 089957@mail.fju.edu.tw Department of Physics, Fu Jen Catholic University, New Taipei City 24205, Taiwan.
Color versions of one or more of the figures in the article can be found online at www.tandfonline.com/list.

carbohydrates is related to several diseases including cancer, and as a result, they are believed to be important drug candidates.[15–17]

In modern glycobiology, it remains a big challenge to fully characterize a variety of carbohydrates and their binding partners because of several reasons. First, the structures of carbohydrates are usually complex, diverse, and heterogeneous.[18,19] Carbohydrate molecules (monosaccharides, oligosaccharides, and polysaccharides) consist of different numbers of sugar units, ranging from one to as many as 500,000 monosaccharide units. Second, unlike nucleic acids and proteins, the synthesis of carbohydrates is not template driven, meaning that multiple enzymes are required in a complex pathway of biosynthesis. Third, the interactions between carbohydrates and other biomolecules are usually of low affinities. For example, due to shallow binding pockets of lectins (carbohydrate-binding proteins), the affinities of these proteins to carbohydrates vary over a wide range (equilibrium dissociation constant ~10^{-3} to 10^{-6} M)[20,21] and are relatively weak compared with antibody–antigen reactions (equilibrium dissociation constant ~10^{-8} to 10^{-12} M).[22,23] Finally, many important functions and roles of carbohydrates have not been fully understood. Comparing to genomics and proteomics, the area of glycomics has just been actively studied in recent years.

To overcome this challenge, modern technologies for glycomics have been proposed and developed,[24,25] including carbohydrate microarrays and label-free biosensors. Microarrays are high-throughput platforms for parallel assays of hundreds to thousands of distinct biomolecular interactions.[26,27] Following the successful development and progress in DNA microarrays[28,29] and protein microarrays,[30,31] carbohydrate microarrays have also become valuable tools in glycobiology.[13,32–34] Carbohydrate microarrays, consisting of distinct glycans immobilized on solid substrates, serve for simultaneously detecting binding reactions of proteins, viruses, and cells to a large number of glycans under identical conditions. There are several ways to efficiently immobilize mono-, di-, oligo-, and polysaccharides on functionalized solid substrates while maintaining their innate functionalities.[35]

For example, unmodified carbohydrates can be directly immobilized on either hydrazide-coated glass slides[36] or nitrocellulose-coated glass slides.[37] Amine- and maleimide-modified carbohydrates can be covalently attached on *N*-hydroxysuccinimide- and thiol-activated glass slides, respectively.[38,39] Traditionally, characterization of bindings between surface-immobilized carbohydrates and solution-phase probes involves some forms of fluorescence-based methods where probes are labeled with fluorescent tags.[38,40,41] However, labeling probes, especially proteins, inevitably changes their binding properties in uncharacterized ways.[42,43] Therefore, a number of label-free, optical biosensors based on surface plasma resonance[44,45] and ellipsometry[46,47] have been developed for measurements of carbohydrate–biomolecule interactions in a high-throughput manner. We recently

developed the oblique-incidence reflectivity difference (OI-RD) microscopy for label-free detection of biomolecular interactions between solution-phase analyte and surface-immobilized microarrays.[48–50] This ellipsometry-based OI-RD microscope is suitable for both real-time measurements of binding curves and end-point imaging of biomolecular microarrays.[51,52]

Bifidobacterium longum subsp. *infantis* (*B. infantis*), one of the earliest colonizers of the gastrointestinal tract of infants, is characterized by its foraging capacity of human milk oligosaccharides.[53] The building blocks of human milk oligosaccharides contain D-glucose, D-galactose, *N*-acetylglucosamine, L-fucose, and sialic acid.[54] To utilize these carbon sources, *B. infantis* has specific glycoside hydrolases to promote the hydrolysis of glycosidic bonds in complex carbohydrates and the following import of these processed glycans. The genome sequence of *B. infantis* showed an overabundance of the Family 1 of solute binding proteins, a portion of bacterial adenosine triphosphate (ATP)-binding cassette transporters (the so-called ABC transporters) and related to the processing of oligosaccharides.[53] Therefore, the characterization of these solute-binding proteins, especially in their interactions with human milk oligosaccharides, is crucial to understanding the molecular mechanisms involved in the adaptations of *B. infantis* to the gastrointestinal tract of infants.

In this paper, we report the characterization of these oligosaccharide-binding proteins using the combination of carbohydrate microarrays and OI-RD microscopy. Twelve human milk oligosaccharides with different mass to charge (m/z) ratios were profiled and separated using the high-performance liquid chromatography–mass spectrometry chip technology described in the literature.[55,56] These human milk oligosaccharides, together with four control oligosaccharides, were aminated for immobilization on epoxy-coated glass substrates as carbohydrate microarrays. These microarrays were further reacted with *B. infantis* Family 1 of solute-binding proteins for determining the binding affinities of specific protein–oligosaccharide interactions. The results indicate that Family 1 of solute-binding proteins has different affinities to host oligosaccharides, and these preferences are important in characterizing the complex process of human milk oligosaccharides foraging by *B. infantis*.

Experimental

Aminated oligosaccharides

Eight human milk oligosaccharides (#1 through #8) with different m/z (mass to charge) ratios were analyzed and separated from human milk oligosaccharides as described in the literature.[55,56] Four known oligosaccharides were purchased from Sigma-Aldrich (St. Louis, MO) (#9, #10, and #12) and Dextra Laboratories Ltd (Reading, UK) (#11). All oligosaccharides were aminated and dissolved in 1× phosphate-buffered saline as targets for microarray printing. The mass (aminated and neutral m/z ratios) and composition (numbers of

hexose, *N*-acetylhexosamine, deoxyhexose, and *N*-acetylneuraminic acid groups) of these aminated oligosaccharides were analyzed by mass spectrometry and the results are listed in Table 1.

Preparation of carbohydrate microarrays and procedure of subsequent reactions

Twelve aminated oligosaccharides were dissolved in 1× phosphate-buffered saline to 100 μM for microarray printing. Using an OmniGrid 100 contact-printing arrayer (Digilab, Inc., Marlborough, MA), two copies of each of the 12 oligosaccharides were immobilized on epoxy-coated glass slides (CEL Associates, Pearland, TX). By contact printing 10 times at each location, a sufficient volume of target solution was deposited over an area of around 100 μM in diameter. The microarray-bearing slides were stored as printed in slide boxes for at least 24 hr before further processing. Subsequently, the slide was assembled into a flow cell and washed with a flow of 1× phosphate-buffered saline for 5 min. To block the remaining free epoxy groups on the glass surface from nonspecific reactions with protein probes, the printed microarray was treated with a flow of bovine serum albumin solution at 8.3 μM in 1× phosphate-buffered saline for 10 min and then washed with a flow of 1× phosphate-buffered saline for 5 min. The 1× phosphate-buffered saline buffer in the flow cell was replaced with a solution of protein probes at a desired concentration for the association phase, and finally the solution was switched back to 1× phosphate-buffered saline buffer for the dissociation phase.

Protein probes

Family 1 of solute-binding proteins from *B. infantis* was cloned and expressed as described in details by Garrido et al.[53] and Kim et al.[57] Six glutathione

Table 1. Mass and composition of the aminated oligosaccharides.

Carbohydrate number	Aminated *m/z*	Neutral *m/z*	Number of hexoses	Number of *N*-acetylhexosamines	Number of deoxyhexoses	Number of *N*-acetylneuraminic acids
1	774.3203	707.2484	3	1		
2	920.3782	853.3063	3	1	1	
3	1139.4525	1072.3806	4	2		
4	1285.5104	1218.4385	4	2	1	
5	1577.6262	1510.5543	4	2	3	
6	1650.6426	1583.5707	5	3	1	
7	2161.8327	2094.7608	6	4	2	
8	2307.8906	2240.8187	6	4	3	
9	694.3206	627.2487		3		
10	700.2836	633.2116	2			1
11	1057.3994	990.3275	6			
12	1219.4522	1152.3803	7			

S-transferase-tagged Family 1 of solute-binding proteins with different genome sequences were dissolved in 1× phosphate-buffered saline to desired concentrations and reacted with the human milk oligosaccharide microarray. The molecular weight of these glutathione *S*-transferase-tagged proteins was estimated to be around 125 kDa (95 kDa for protein +30 kDa for glutathione *S*-transferase tag).

OI-RD microscopy for label-free carbohydrate microarray detection

The OI-RD scanning microscope used in the present work was described in earlier publications.[42,51,52] It used a He–Ne laser at a wavelength of 633 nM for illumination. We measured the OR-RD signal defined as $(r_p - r_{p0})/r_{p0} - (r_s - r_{s0})/r_{s0} \equiv \Delta_p - \Delta_s$, where r_{p0} and r_{s0} are the complex reflectivities of the bare glass surface, r_p and r_s are the reflectivities of the glass surface covered with immobilized carbohydrate layer.[58] The physical properties of a surface-bound biomolecular layer are related to $\Delta_p - \Delta_s$ by[50,59]:

$$\Delta_p - \Delta_s \cong -i\left[\frac{4\pi\varepsilon_s(\tan\phi_{inc})^2\cos\phi_{inc}}{\varepsilon_0^{1/2}(\varepsilon_s - \varepsilon_0)\left(\varepsilon_s/\varepsilon_0 - (\tan\phi_{inc})^2\right)}\right]\frac{(\varepsilon_d - \varepsilon_s)(\varepsilon_d - \varepsilon_0)\Theta}{\varepsilon_d}\left(\frac{d}{\lambda}\right),$$

where ϕ_{inc} is the incidence angle of the illumination laser beam, and ε_0, ε_d, and ε_s are the respective optical constants of the aqueous ambient, biomolecular layer (e.g., printed targets and/or captured probes), and glass slide at 633 nM. In our present study, $\phi_{inc} = 65°$, $\varepsilon_s = 2.307$ for glass slide, $\varepsilon_0 = 1.788$ for aqueous buffer, and $\varepsilon_d = 2.031$ for packed biomolecules in solution.[50] In this work, d is the thickness of the biomolecular layer and Θ is the coverage of the layer, defined as the ratio of the area covered by the layer to the total available area. Θd and thus $\Delta_p - \Delta_s$ is proportional to the surface mass density (Γ) of the immobilized molecular layer.

The OI-RD image of a carbohydrate microarray was acquired by moving the sample stage two dimensionally with a linear step size of 20 μM in both directions. To acquire real-time binding curves, we measured the OI-RD signals of one pixel from a printed spot (target pixel) and one pixel from the unprinted region adjacent to the target (reference pixel), and took the difference as one time point of the binding curve. This was repeated at a time interval shorter than the characteristic time of the reaction. This procedure reduced the contribution of drift in the optical system to the binding curve measurement.

Model for analysis of binding curves

Rate constants and equilibrium dissociation constants for protein–carbohydrate interactions were deduced by globally fitting a set of binding curves, each of which corresponded to a concentration [c] of the protein, to the 1-to-1 Langmuir reaction model.[45,60,61] In this model, the surface mass

density $\Gamma(t)$ of the captured protein evolves during the association phase of the binding reaction as follows:

$$\Gamma(t) = \frac{\Gamma_{MAX} k_{on}[c]}{k_{on}[c] + k_{off}} \left(1 - e^{-(k_{on}[c]+k_{off})t}\right) \quad 0 < t < t_0; \tag{2}$$

during the subsequent dissociation phase, i.e., after the probe solution is replaced with 1× phosphate-buffered saline buffer at $t = t_0$,

$$\Gamma(t) = \frac{\Gamma_{MAX} k_{on}[c]}{k_{on}[c] + k_{off}} \left(1 - e^{-(k_{on}[c]+k_{off})t_0}\right) e^{-k_{off}(t-t_0)} \quad t > t_0. \tag{3}$$

where Γ_{MAX} is the maximum amount of probes that can be captured by the immobilized carbohydrate targets, and k_{on} and k_{off} are the association and dissociation rate constants, respectively. The equilibrium dissociation constant of a binding reaction is defined as $K_D = k_{off}/k_{on}$. Since the OI-RD signal [Eq. (1)] is proportional to $\Gamma(t)$, we expect the optical signal to vary in time as:

$$\Delta_p - \Delta_s = \gamma \frac{k_{on}[c]}{k_{on}[c] + k_{off}} \left(1 - e^{-(k_{on}[c]+k_{off})t}\right) \quad \text{(Association) } 0 < t < t_0; \tag{4}$$

$$\Delta_p - \Delta_s = \gamma \frac{k_{on}[c]}{k_{on}[c] + k_{off}} \left(1 - e^{-(k_{on}[c]+k_{off})t_0}\right) e^{-k_{off}(t-t_0)} \quad \text{(Dissociation) } t > t_0. \tag{5}$$

Here, γ, one of the fitting parameters, is proportional to Γ_{MAX}.

Results and discussion

OI-RD images of carbohydrate microarrays

Figure 1 shows the OI-RD image of a carbohydrate microarray after printing. The spot size is approximately 100 μM in diameter, and the center-to-center spacing is about 200 μM. The corresponding layout of the microarray is illustrated to the right. The intensity bar is not shown because the OI-RD signals of this dry microarray are oversaturated due to surface-accumulated salts and excess oligosaccharide targets. To remove these precipitates, the microarray was first washed with 1× phosphate-buffered saline. The OI-RD image of the carbohydrate microarray after washing is shown in Figure 2a (with the microarray still in contact with 1× phosphate-buffered saline). After washing, all target spots are visible with OI-RD signals of 1×10^{-3} to 2×10^{-3}. These correspond to surface mass densities Γ of 1.7×10^{-7} to 3.4×10^{-7} g/cm^2[51] and the microarray was blocked with a bovine serum albumin solution of 8.3 μM for 10 min. Figure 2b shows the differential OI-RD image of the microarray, obtained by subtracting the image taken after washing from the image taken after blocking and subsequent washing (with the microarray still

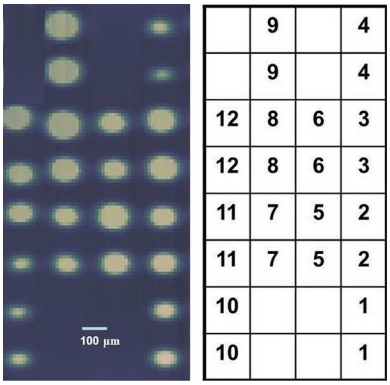

Figure 1. OI-RD image and corresponding layout of the dry carbohydrate microarray. *Note*: OI-RD, oblique-incidence reflectivity difference.

in contact with 1× phosphate-buffered saline). After blocking, free bovine serum albumin molecules bound to unprinted regions, and all target spots became darker as a result of an increased background signal. It has been shown that under this blocking concentration (8.3 μM of bovine serum albumin), a side-on monolayer of fully packed bovine serum albumin molecules ($\Gamma \sim 4 \times 10^{-7}$ g/cm^2) was accumulated on the surface.[51] Therefore, all surface-immobilized oligosaccharides must have less than a side-on monolayer of fully packed bovine serum albumin molecules.

Binding kinetics of solute-binding proteins to oligosaccharides

The carbohydrate microarray containing 12 oligosaccharides was reacted with six different Family 1 of solute-binding proteins at desired concentrations.

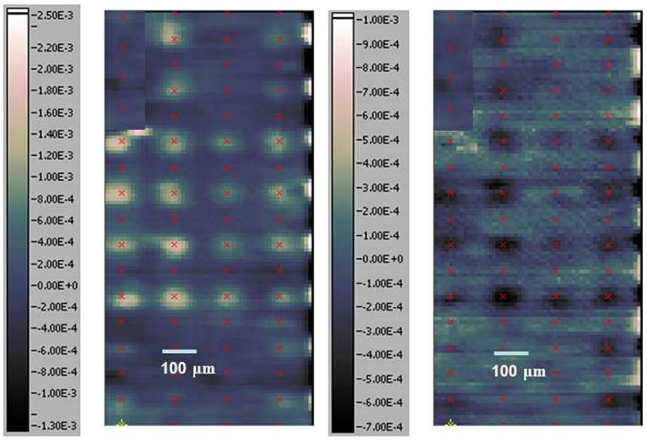

Figure 2. (a) OI-RD image of the carbohydrate microarray in contact with 1× phosphate-buffered saline buffer and (b) differential OI-RD image of the microarray after blocking. *Note*: OI-RD, oblique-incidence reflectivity difference.

One fresh microarray was used in each reaction condition (one protein at one concentration). Figure 3 shows the association–dissociation curves for solute-binding protein 2344 reacting with 12 oligosaccharides. The concentrations of proteins are 236 (red), 472 (green), and 944 (blue) nM. At $t = 0$, the aqueous ambient in contact with the microarray was changed from 1× phosphate buffered saline to a protein solution at a desired concentration. At $t = 1{,}800$ s,

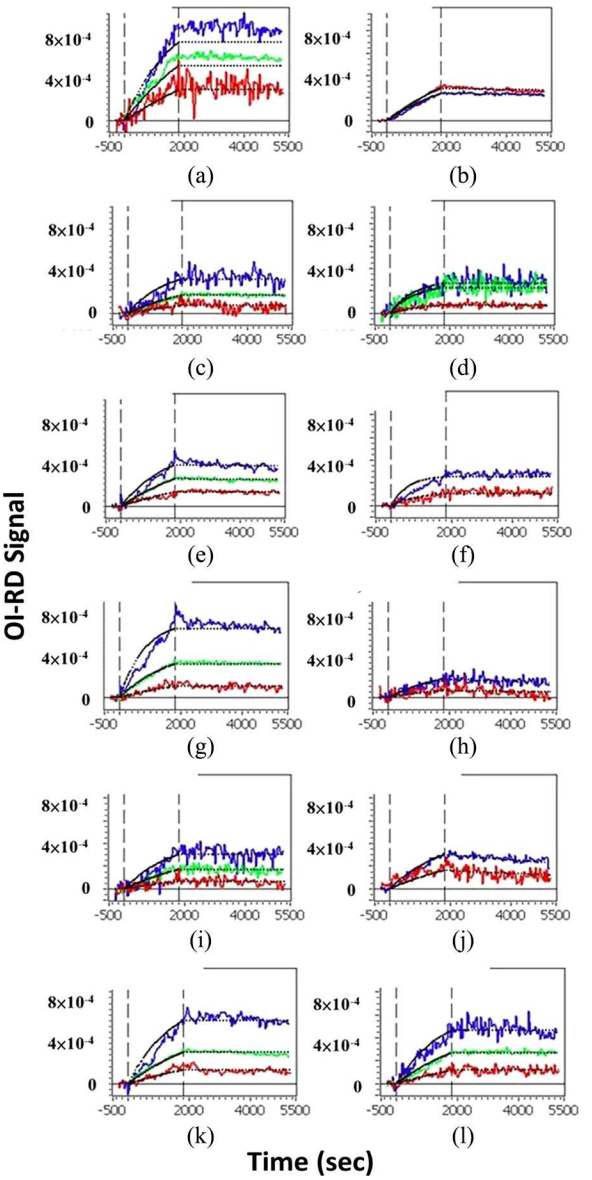

Figure 3. Association–dissociation curves of solute-binding protein 2344 reacting with the surface-immobilized oligosaccharides: (a) #1; (b) #2; (c) #3; (d) #4; (e) #5; (f) #6; (g) #7; (h) #8; (i) #9; (j) #10; (k) #11; and (l) # 12. The colors indicate different probe concentrations—red: 236 nM; green: 472 nM; and blue: 944 nM.

the ambient was restored back to 1× phosphate-buffered saline for dissociation. The binding curves in each panel were fitted globally to the 1-to-1 Langmuir reaction model [Eqs. (4) and (5)] with k_{on}, k_{off}, and γ being the global fitting parameters. The fits are shown in dotted lines in the figure and the equilibrium dissociation constants are listed in Table 2.

From Figure 3, it is clear that solute-binding protein 2344 reacted with all 12 oligosaccharides, but the OI-RD signals were relatively weak (1×10^{-4} to 8×10^{-4}) compared with those of printed targets (1×10^{-3} to 2×10^{-3}). These signals correspond to only about one-tenth of a side-on monolayer of fully packed immunoglobulin G molecules (an antibody isotype with a molecular weight of 150 kDa).[51] Also, except for #2, #8, and #10, the dissociation phase was not obvious so that dissociation rate constants and equilibrium dissociation constants have no values but only upper limits.[51,62] For example, the equilibrium dissociation constant of solute-binding protein 2344 binding to #1 is less than 42 nM. In summary, the equilibrium dissociation constants of solute-binding protein 2344 binding to oligosaccharides range from 6 nM (#6, the strongest binding affinity) to 79 nM (#10, the weakest binding affinity), and these values are close to what have been reported in lectin–oligosaccharide reactions.[62]

Figures 4–8 show the association–dissociation curves of 12 oligosaccharides reacting with solute-binding protein 2352, solute-binding protein 2350, solute-binding protein 0343, solute-binding protein 2177, and solute-binding protein 0883, respectively. The colors indicate different probe concentrations as reported in the figure captions. After globally fitting the curves in each

Table 2. Equilibrium dissociation constants in nM of solute-binding proteins binding to carbohydrates. Numbers in the solute-binding proteins represent each Family 1 of the solute-binding protein locus tag.

Carbohydrate number (first column)/ solute-binding protein (first row)/ equilibrium dissociation constant (nM)	2344	2352	2350	0343	2177	0883
1	<42 ± 2.1	<11.1 ± 0.9	<96.5 ± 5.2	37.4 ± 2.2	69.9 ± 5.1	8.85 ± 1.2
2	22.6 ± 1.5	No reaction	75.2 ± 6.2	52.4 ± 3.2	No reaction	225 ± 10.3
3	<57.7 ± 6.1	No reaction	71 ± 5.2	18.7 ± 2.5	No reaction	62.6 ± 7.1
4	<19.2 ± 1.1	No reaction	No reaction	41.8 ± 3.6	<2.97 ± 0.8	No reaction
5	<15.4 ± 0.9	<17.5 ± 1.2	64.34 ± 8.2	66.7 ± 7.1	No reaction	No reaction
6	<5.97 ± 1.0	<24 ± 3.1	<86.4 ± 7.6	72.1 ± 5.9	No reaction	35.3 ± 4.1
7	<16.3 ± 2.0	148 ± 11.1	12.1 ± 2.0	41.3 ± 3.8	No reaction	26.8 ± 3.0
8	68.7 ± 6.2	No reaction	No reaction	No reaction	No reaction	No reaction
9	<66 ± 5.9	<58.5 ± 6.0	<21.5 ± 1.9	28.6 ± 3.0	No reaction	189 ± 12.9
10	78.7 ± 8.0	51.6 ± 5.8	173 ± 12.2	11.6 ± 2.0	3.26 ± 0.8	35.5 ± 4.1
11	<22.7 ± 2.2	<13.7 ± 2.0	38.4 ± 4.1	19.5 ± 1.4	No reaction	No reaction
12	<30.5 ± 2.5	<13.4 ± 2.1	<70.2 ± 6.5	8.18 ± 1.1	No reaction	No reaction

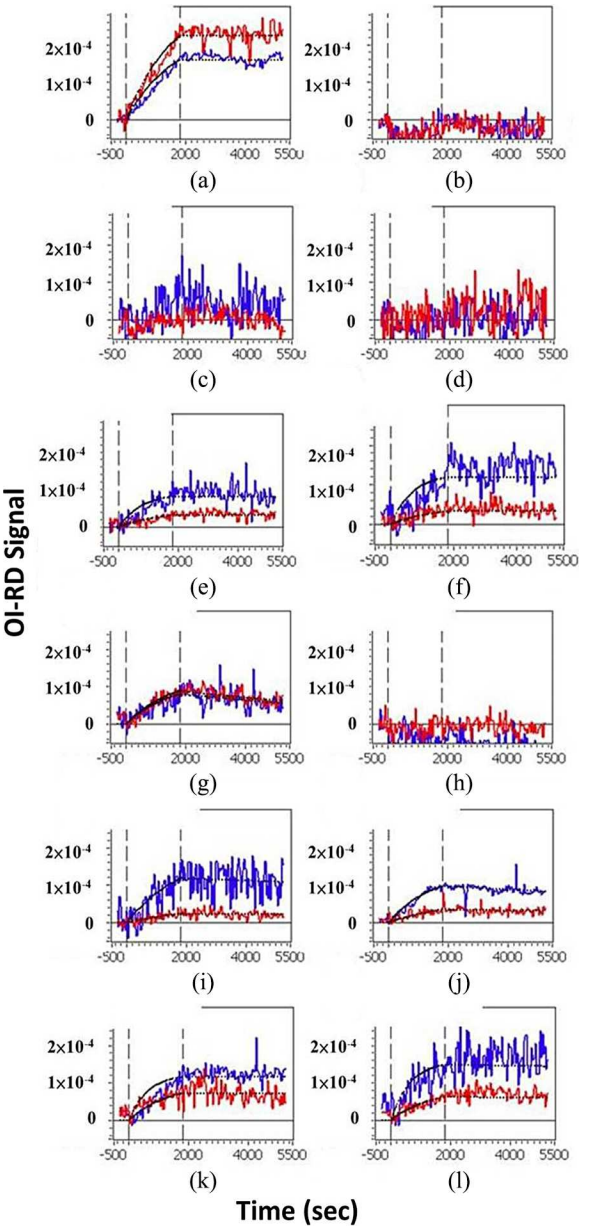

Figure 4. Association–dissociation curves of solute-binding protein 2352 reacting with the surface-immobilized oligosaccharides: (a) #1; (b) #2; (c) #3; (d) #4; (e) #5; (f) #6; (g) #7; (h) #8; (i) #9; (j) #10; (k) #11; and (l) #12. The colors indicate different probe concentrations—red: 400 nM and blue: 800 nM.

panel, the equilibrium dissociation constants of all reactions are listed in Table 2. Solute-binding protein 2352 reacted with #1, #5, #6, #7, #9, #10, #11, and #12 with small OI-RD signals (1×10^{-4} to 2×10^{-4}, corresponding to about one-thirtieth of a side-on monolayer of fully packed immunoglobulin G molecules). It has the strongest binding affinity (the smallest equilibrium

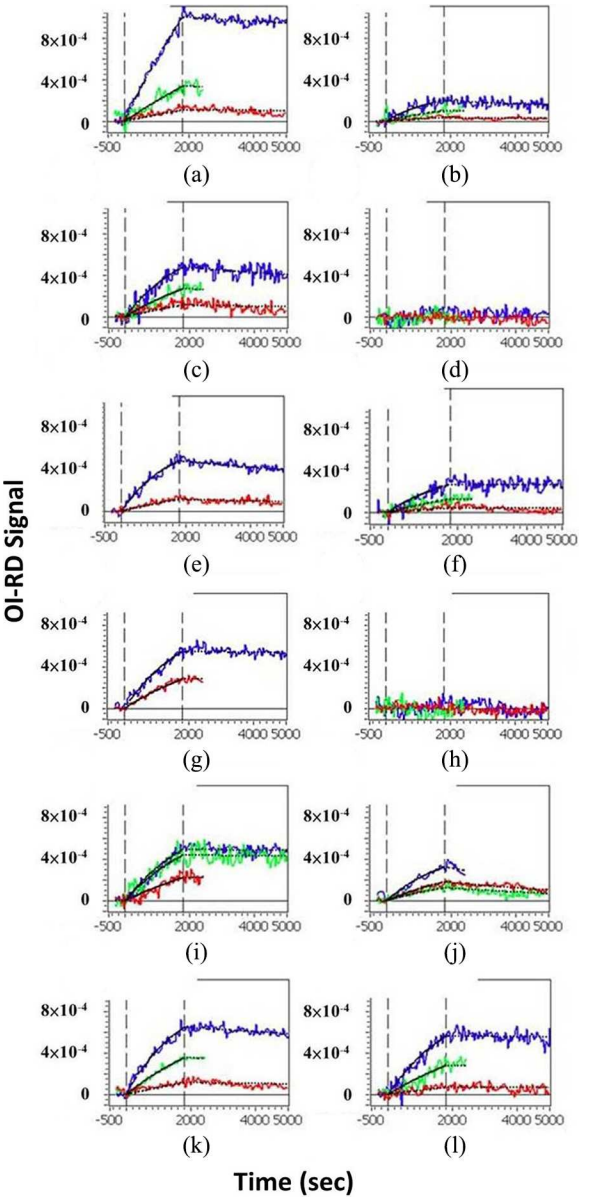

Figure 5. Association–dissociation curves of solute-binding protein 2350 reacting with the surface-immobilized oligosaccharides: (a) #1; (b) #2; (c) #3; (d) #4; (e) #5; (f) #6; (g) #7; (h) #8; (i) #9; (j) #10; (k) #11; and (l) #12. The colors indicate different probe concentrations—red: 170 nM; green: 340 nM; and blue: 680 nM.

dissociation constant for 11 nM) to #1 and the weakest binding affinity (the largest equilibrium dissociation constant of approximately 150 nM) to #7. Solute-binding protein 2350 reacted with #1, #2, #3, #5, #6, #7, #9, #10, #11, and #12 with OI-RD signals of 1×10^{-4} to 8×10^{-4} (corresponding to approximately one-tenth of a side-on monolayer of fully packed immunoglobulin G molecules).

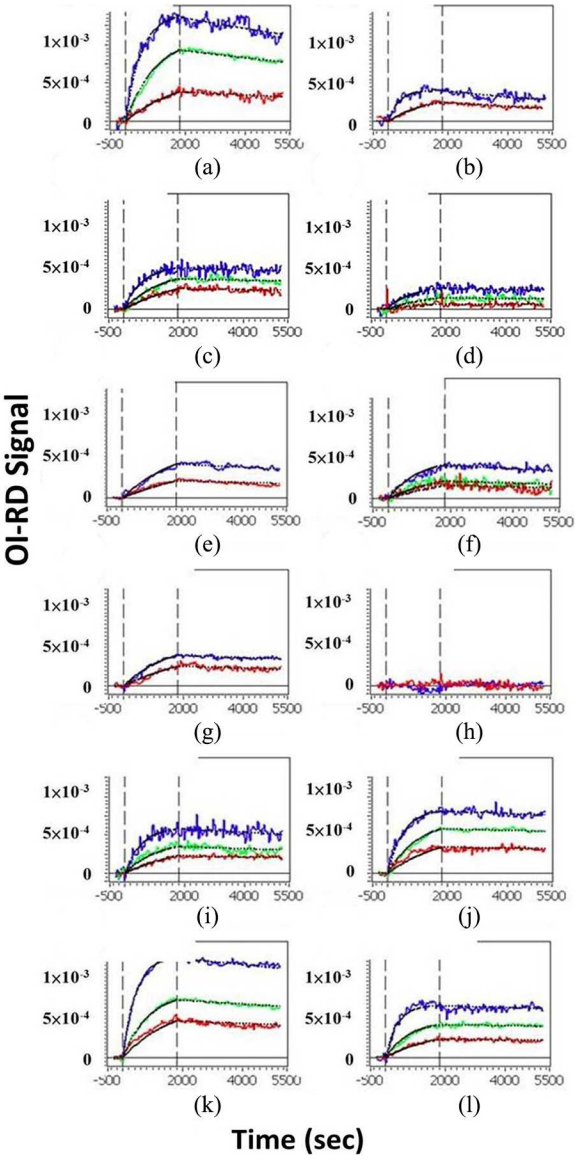

Figure 6. Association–dissociation curves of solute-binding protein 0343 reacting with the surface-immobilized oligosaccharides: (a) #1; (b) #2; (c) #3; (d) #4; (e) #5; (f) #6; (g) #7; (h) #8; (i) #9; (j) #10; (k) #11; and (l) #12. The colors indicate different probe concentrations—red: 340 nM; green: 680 nM; and blue: 1,360 nM.

As shown in Figure 5, some dissociation curves were missing due to large drift in this set of reactions. It has the strongest binding affinity (the smallest equilibrium dissociation constant of 12 nM) to #7 and the weakest binding affinity (the largest equilibrium dissociation constant of 173 nM) to #10. Solute-binding protein 0343 reacted with all oligosaccharides except #8 with relatively higher OI-RD signals (up to 2×10^{-3}, corresponding to about one-half of a side-on monolayer of fully packed immunoglobulin

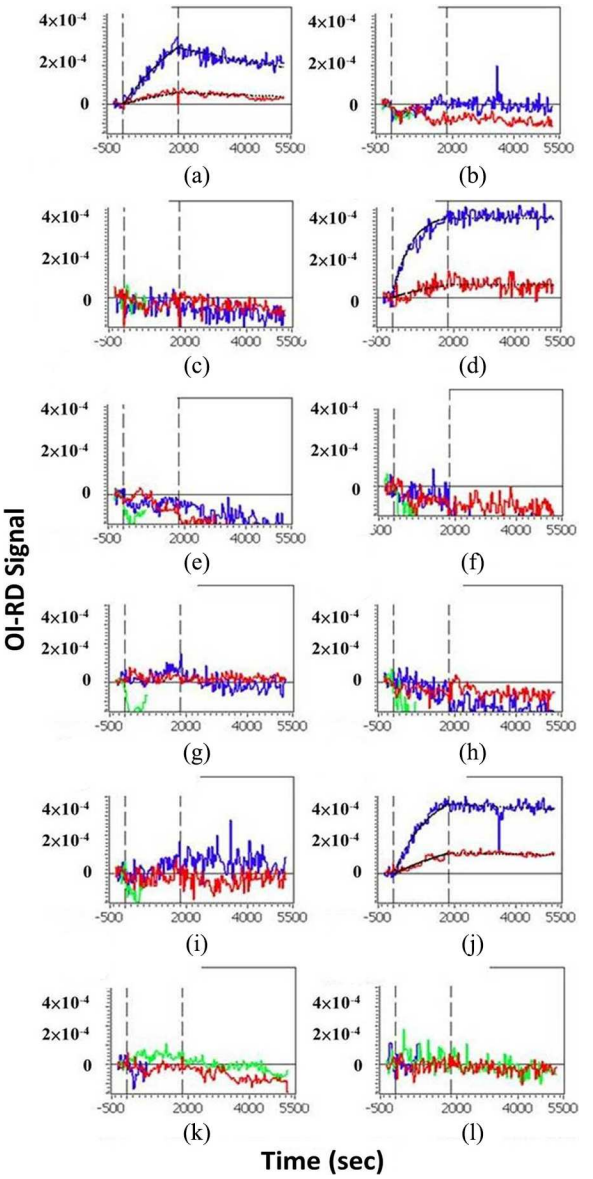

Figure 7. Association–dissociation curves of solute-binding protein 2177 reacting with the surface-immobilized oligosaccharides: (a) #1; (b) #2; (c) #3; (d) #4; (e) #5; (f) #6; (g) #7; (h) #8; (i) #9; (j) #10; (k) #11; and (l) #12. The colors indicate different probe concentrations—red: 29 nM; green: 57 nM; and blue: 114 nM.

G molecules). It has the strongest binding affinity (the smallest equilibrium dissociation constant of 8 nM) to #12 and the weakest binding affinity (the largest equilibrium dissociation constant of 72 nM) to #6.

Solute-binding protein 2177 reacted only with #1, #4, and #10 with OI-RD signals of 1×10^{-4} to 4×10^{-4} (corresponding to about one-twentieth of a side-on monolayer of fully packed immunoglobulin G molecules). It has the

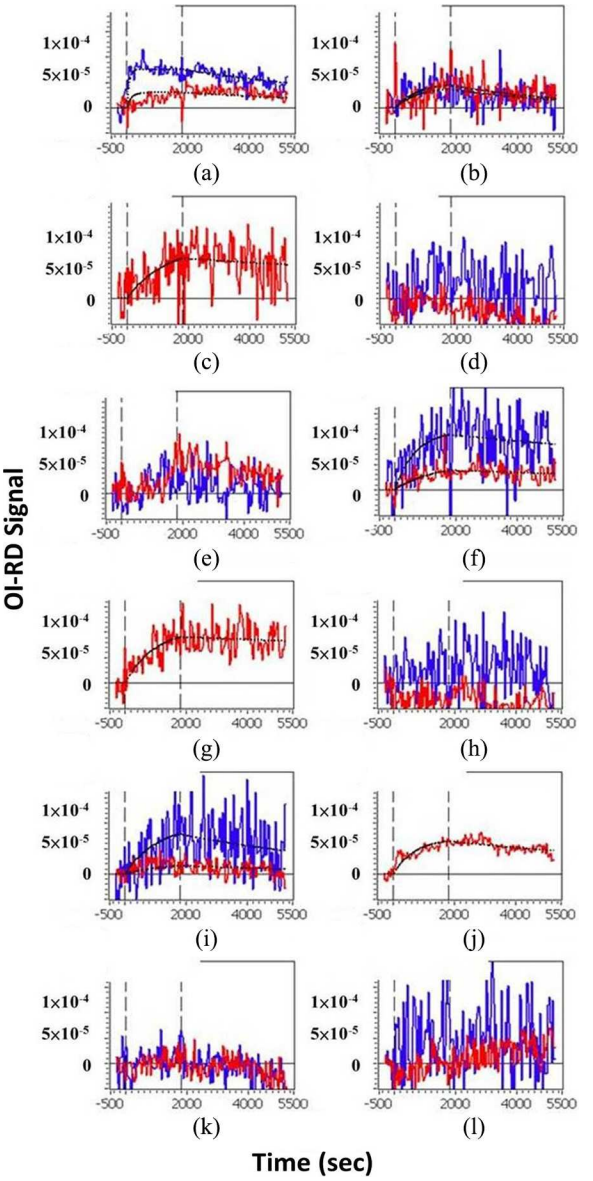

Figure 8. Association–dissociation curves of solute binding protein 0883 reacting with the surface-immobilized oligosaccharides: (a) #1; (b) #2; (c) #3; (d) #4; (e) #5; (f) #6; (g) #7; (h) #8; (i) #9; (j) #10; (k) #11; and (l) #12. The colors indicate different probe concentrations—red: 474 nM and blue: 948 nM.

strongest binding affinity (the smallest equilibrium dissociation constant of 3 nM) to #4 and #10, and the weakest binding affinity (the largest equilibrium dissociation constant of 70 nM) to #1. Solute-binding protein 0883 reacted with #1, #2, #3, #6, #7, #9, and #10 with weak OI-RD signals (less than 1×10^{-4}, corresponding to about one-fortieth of a side-on monolayer of fully packed immunoglobulin G molecules). It has the strongest binding affinity

(the smallest equilibrium dissociation constant of 9 nM) to #1 and the weakest binding affinity (the largest equilibrium dissociation constant of 225 nM) to #2.

From Figures 3–8 and Table 2, oligosaccharide-binding proteins Family 1 of solute binding proteins from *B. infantis* show specific preferences for host glycans. These protein–oligosaccharide interactions have different binding intensities (different OI-RD signals) and affinities (different equilibrium dissociation constants). The next step will be to study the dependence of these preferences on the structures of surface-immobilized oligosaccharides. This will help in characterizing the complex process of oligosaccharides, particularly human milk oligosaccharides, foraging by *B. infantis*.

Conclusions

Carbohydrate microarrays are high-throughput assay platforms for characterizing and profiling protein–carbohydrate interactions that are numerous and complex. Label-free, real-time, and *in situ* detection of protein-binding reactions with carbohydrate microarrays have advantages over fluorescence-based methods by preserving the innate properties of proteins and offering the capability of measuring association–dissociation curves and thus directly yielding reaction kinetics. The latter not only enhances the efficiency and relevance of carbohydrate microarray platforms but also makes the platform free of density variation of immobilized targets. Using the OI-RD scanning microscope as a versatile label-free biosensor of carbohydrate microarrays, we characterized different oligosaccharide-binding proteins by studying their binding affinities to surface-immobilized glycans including human milk oligosaccharides. We found that Family 1 of solute-binding proteins from *B. infantis* reveals preferences for host oligosaccharides, and the structural difference in carbohydrates can induce large changes in binding affinity constants in terms of equilibrium dissociation constant. Therefore, the combination of a label-free OI-RD biosensor and carbohydrate microarrays can be utilized to profile and characterize selected proteins and their interactions with glycans.

Acknowledgments

The authors want to thank to Dr. David A. Mills for providing the protein probes and Dr. Carlito Lebrilla for providing the oligosaccharides.

Funding

This work was financially supported by NIH-R01-HG003827 (X. D. Zhu) and Taiwan MOST 105-2112-M-030-002-MY2 (Y.-S. Sun).

References

[1] Roseman, S. Reflections on Glycobiology. *J. Biol. Chem.* **2001**, *276*(45), 41527–41542.

[2] Horlacher, T.; Seeberger, P. H. Carbohydrate Arrays as Tools for Research and Diagnostics. *Chem. Soc. Rev.* **2008**, *37*(7), 1414–1422.

[3] Adachi, T.; Sato, C.; Kishi, Y.; Totani, K.; Murata, T.; Usui, T.; Kitajima, K. Membrane Microdomains from Early Gastrula Embryos of Medaka, *Oryzias latipes*, are a Platform of E-cadherin- and Carbohydrate-mediated Cell–Cell Interactions During Epiboly. *Glycoconjuate J.* **2009**, *26*(3), 285–299.

[4] Crocker, P. R.; Feizi, T. Carbohydrate Recognition Systems: Functional Triads in Cell–Cell Interactions. *Curr. Opin. Struct. Biol.* **1996**, *6*(5), 679–691.

[5] Miura, R.; Ethell, I. M.; Yamaguchi, Y. Carbohydrate-protein Interactions Between HNK-1-reactive Sulfoglucuronyl Glycolipids and the Proteoglycan Lectin Domain Mediate Neuronal Cell Adhesion and Neurite Outgrowth. *J. Neurochem.* **2001**, *76*(2), 413–424.

[6] Lorenz, B.; Alvarez de Cienfuegos, L.; Oelkers, M.; Kriemen, E.; Brand, C.; Stephan, M.; Sunnick, E.; Yuksel, D.; Kalsani, V.; Kumar, K.; Werz, D. B.; Janshoff, A. Model System for Cell Adhesion Mediated by Weak Carbohydrate–Carbohydrate Interactions. *J. Am. Chem. Soc.* **2012**, *134*(7), 3326–3329.

[7] Kahsai, A. W.; Cui, J.; Kaniskan, H. U.; Garner, P. P.; Fenteany, G. Analogs of Tetrahydroisoquinoline Natural Products that Inhibit Cell Migration and Target Galectin-3 Outside of its Carbohydrate-binding Site. *J. Biol. Chem.* **2008**, *283*(36), 24534–24545.

[8] Chou, D. K.; Zhang, J.; Smith, F. I.; McCaffery, P.; Jungalwala, F. B. Developmental Expression of Receptor for Advanced Glycation End Products (RAGE), Amphoterin and Sulfoglucuronyl (HNK-1) Carbohydrate in Mouse Cerebellum and Their Role in Neurite Outgrowth and Cell Migration. *J. Neurochem.* **2004**, *90*(6), 1389–1401.

[9] Krishnan, V.; Bane, S. M.; Kawle, P. D.; Naresh, K. N.; Kalraiya, R. D. Altered Melanoma Cell Surface Glycosylation Mediates Organ Specific Adhesion and Metastasis Via Lectin Receptors on the Lung Vascular Endothelium. *Clin. Exp. Metastasis* **2005**, *22*(1), 11–24.

[10] Ruseva, M.; Kolev, M.; Dagnaes-Hansen, F.; Hansen, S. B.; Takahashi, K.; Ezekowitz, A.; Thiel, S.; Jensenius, J. C.; Gadjeva, M. Mannan-binding Lectin Deficiency Modulates the Humoral Immune Response Dependent on the Genetic Environment. *Immunology* **2009**, *127*(2), 279–288.

[11] Lackie, A. M.; Vasta, G. R. The Role of Galactosyl-binding Lectin in the Cellular Immune Response of the Cockroach *Periplaneta americana* (Dictyoptera). *Immunology* **1988**, *64*(2), 353–357.

[12] Schauer, R. *Sialic Acids, Chemistry, Metabolism and Function*. Springer-Verlag: New York, 1982; Vol. 10.

[13] Stevens, J.; Blixt, O.; Glaser, L.; Taubenberger, J. K.; Palese, P.; Paulson, J. C.; Wilson, I. A. Glycan Microarray Analysis of the Hemagglutinins from Modern and Pandemic Influenza Viruses Reveals Different Receptor Specificities. *J. Mol. Biol.* **2006**, *355*(5), 1143–1155.

[14] Smith, A. E.; Helenius, A. How Viruses Enter Animal Cells. *Science* **2004**, *304*(5668), 237–242.

[15] Liu, C. C.; Ye, X. S. Carbohydrate-based Cancer Vaccines: Target Cancer with Sugar Bullets. *Glycoconjugate J.* **2012**, *29*(5–6), 259–271.

[16] Adamo, R.; Nilo, A.; Harfouche, C.; Brogioni, B.; Pecetta, S.; Brogioni, G.; Balducci, E.; Pinto, V.; Filippini, S.; Mori, E.; Tontini, M.; Romano, M. R.; Costantino, P.; Berti, F. Investigating the Immunodominance of Carbohydrate Antigens in a Bivalent

Unimolecular Glycoconjugate Vaccine Against Serogroup A and C Meningococcal Disease. *Glycoconjugate J.* **2014**, *31*(9), 637–647.
[17] Seeberger, P. H.; Werz, D. B. Automated Synthesis of Oligosaccharides as a Basis for Drug Discovery. *Nat. Rev. Drug Discovery* **2005**, *4*(9), 751–763.
[18] Wang, D. Carbohydrate Microarrays. *Proteomics* **2003**, *3*(11), 2167–2175.
[19] Imai, Y.; Rosen, S. D. Direct Demonstration of Heterogeneous, Sulfated *O*-linked Carbohydrate Chains on an Endothelial Ligand for L-selectin. *Glycoconjugate J.* **1993**, *10*(1), 34–39.
[20] Shinohara, Y.; Hasegawa, Y.; Kaku, H.; Shibuya, N. Elucidation of the Mechanism Enhancing the Avidity of Lectin with Oligosaccharides on the Solid Phase Surface. *Glycobiology* **1997**, *7*(8), 1201–1208.
[21] Lee, Y. C.; Lee, R. T. Carbohydrate-protein Interactions: Basis of Glycobiology. *Acc. Chem. Res.* **1995**, *28*, 321–327.
[22] Papalia, G. A.; Baer, M.; Luehrsen, K.; Nordin, H.; Flynn, P.; Myszka, D. G. High-resolution Characterization of Antibody Fragment/Antigen Interactions using Biacore T100. *Anal. Biochem.* **2006**, *359*(1), 112–119.
[23] Katsamba, P. S.; Navratilova, I.; Calderon-Cacia, M.; Fan, L.; Thornton, K.; Zhu, M.; Bos, T. V.; Forte, C.; Friend, D.; Laird-Offringa, I.; Tavares, G.; Whatley, J.; Shi, E.; Widom, A.; Lindquist, K. C.; Klakamp, S.; Drake, A.; Bohmann, D.; Roell, M.; Rose, L.; Dorocke, J.; Roth, B.; Luginbuhl, B.; Myszka, D. G. Kinetic Analysis of a High-affinity Antibody/Antigen Interaction Performed by Multiple Biacore Users. *Anal. Biochem.* **2006**, *352*(2), 208–221.
[24] Bertozzi, C. R.; Kiessling, L. L. Chemical Glycobiology. *Science* **2001**, *291*(5512), 2357–2364.
[25] Ratner, D. M.; Adams, E. W.; Disney, M. D.; Seeberger, P. H. Tools for Glycomics: Mapping Interactions of Carbohydrates in Biological Systems. *Chembiochem* **2004**, *5*(10), 1375–1383.
[26] Schena, M. *Microarray Analysis*. John Wiley and Sons: Hoboken, NJ, 2003.
[27] MacBeath, G. Protein Microarrays and Proteomics. *Nat. Genet.* **2002**, *32*(Suppl.), 526–532.
[28] Lockhart, D. J.; Winzeler, E. A. Genomics, Gene Expression and DNA Arrays. *Nature* **2000**, *405*(6788), 827–836.
[29] Ramsay, G. DNA Chips: State-of-the Art. *Nat. Biotechnol.* **1998**, *16*(1), 40–44.
[30] Zhu, H.; Bilgin, M.; Bangham, R.; Hall, D.; Casamayor, A.; Bertone, P.; Lan, N.; Jansen, R.; Bidlingmaier, S.; Houfek, T.; Mitchell, T.; Miller, P.; Dean, R. A.; Gerstein, M.; Snyder, M. Global Analysis of Protein Activities using Proteome Chips. *Science* **2001**, *293*(5537), 2101–2105.
[31] MacBeath, G.; Schreiber, S. L. Printing Proteins as Microarrays for High-throughput Function Determination. *Science* **2000**, *289*(5485), 1760–1763.
[32] Liang, P. H.; Wu, C. Y.; Greenberg, W. A.; Wong, C. H. Glycan Arrays: Biological and Medical Applications. *Curr. Opin. Chem. Biol.* **2008**, *12*(1), 86–92.
[33] Huang, C. Y.; Thayer, D. A.; Chang, A. Y.; Best, M. D.; Hoffmann, J.; Head, S.; Wong, C. H. Carbohydrate Microarray for Profiling the Antibodies Interacting with Globo H Tumor Antigen. *Proc. Natl. Acad. Sci. USA* **2006**, *103*(1), 15–20.
[34] Blixt, O.; Head, S.; Mondala, T.; Scanlan, C.; Huflejt, M. E.; Alvarez, R.; Bryan, M. C.; Fazio, F.; Calarese, D.; Stevens, J.; Razi, N.; Stevens, D. J.; Skehel, J. J.; van Die, I.; Burton, D. R.; Wilson, I. A.; Cummings, R.; Bovin, N.; Wong, C. H.; Paulson, J. C. Printed Covalent Glycan Array for Ligand Profiling of Diverse Glycan Binding Proteins. *Proc. Natl. Acad. Sci. USA* **2004**, *101*(49), 17033–17038.

[35] Monzo, A.; Guttman, A. Immobilization Techniques for Mono- and Oligosaccharide Microarrays. *QSAR Comb. Sci.* **2006**, *25*(11), 1033–1038.
[36] Lee, M. R.; Shin, I. Facile Preparation of Carbohydrate Microarrays by Site-specific, Covalent Immobilization of Unmodified Carbohydrates on Hydrazide-coated Glass Slides. *Org. Lett.* **2005**, *7*(19), 4269–4272.
[37] Wang, D.; Liu, S.; Trummer, B. J.; Deng, C.; Wang, A. Carbohydrate Microarrays for the Recognition of Cross-reactive Molecular Markers of Microbes and Host Cells. *Nat. Biotechnol.* **2002**, *20*(3), 275–281.
[38] Liang, P. H.; Wang, S. K.; Wong, C. H. Quantitative Analysis of Carbohydrate-protein Interactions using Glycan Microarrays: Determination of Surface and Solution Dissociation Constants. *J. Am. Chem. Soc.* **2007**, *129*(36), 11177–11184.
[39] Park, S.; Shin, I. Fabrication of Carbohydrate Chips for Studying Protein-carbohydrate Interactions. *Angew. Chem. Int. Ed. Engl.* **2002**, *41*(17), 3180–3182.
[40] Oyelaran, O.; McShane, L. M.; Dodd, L.; Gildersleeve, J. C. Profiling Human Serum Antibodies with a Carbohydrate Antigen Microarray. *J. Proteome Res.* **2009**, *8*(9), 4301–4310.
[41] Manimala, J. C.; Roach, T. A.; Li, Z.; Gildersleeve, J. C. High-throughput Carbohydrate Microarray Profiling of 27 Antibodies Demonstrates Widespread Specificity Problems. *Glycobiology* **2007**, *17*(8), 17C–23C.
[42] Sun, Y. S.; Landry, J. P.; Fei, Y. Y.; Zhu, X. D.; Luo, J. T.; Wang, X. B.; Lam, K. S. Effect of Fluorescently Labeling Protein Probes on Kinetics of Protein-ligand Reactions. *Langmuir* **2008**, *24*(23), 13399–13405.
[43] Kodadek, T. Protein Microarrays: Prospects and Problems. *Chem. Biol.* **2001**, *8*(2), 105–115.
[44] Duverger, E.; Frison, N.; Roche, A. C.; Monsigny, M. Carbohydrate-lectin Interactions Assessed by Surface Plasmon Resonance. *Biochimie* **2003**, *85*(1–2), 167–179.
[45] Nahalkova, J.; Svitel, J.; Gemeiner, P.; Danielsson, B.; Pribulova, B.; Petrus, L. Affinity Analysis of Lectin Interaction with Immobilized C- and O-gylcosides Studied by Surface Plasmon Resonance Assay. *J. Biochem. Biophys. Methods* **2002**, *52*(1), 11–18.
[46] Niu, Y.; Jin, G. Protein Microarray Biosensors based on Imaging Ellipsometry Techniques and Their Applications. *Protein Cell* **2011**, *2*(6), 445–455.
[47] Venkatasubbarao, S.; Beaudry, N.; Zhao, Y.; Chipman, R. Evanescent-imaging-ellipsometry-based Microarray Reader. *J. Biomed. Opt.* **2006**, *11*(1), 014028.
[48] Sun, Y. S.; Zhu, X. Real-time, Label-free Detection of Biomolecular Interactions in Sandwich Assays by the Oblique-incidence Reflectivity Difference Technique. *Sensors (Basel)* **2014**, *14*(12), 23307–23320.
[49] Fei, Y. Y.; Landry, J. P.; Sun, Y. S.; Zhu, X. D.; Luo, J. T.; Wang, X. B.; Lam, K. S. A Novel High-throughput Scanning Microscope for Label-free Detection of Protein and Small-molecule Chemical Microarrays. *Rev. Sci. Instrum.* **2008**, *79*(1), 013708.
[50] Landry, J. P.; Sun, Y. S.; Guo, X. W.; Zhu, X. D. Protein Reactions with Surface-bound Molecular Targets Detected by Oblique-incidence Reflectivity Difference Microscopes. *Appl. Opt.* **2008**, *47*(18), 3275–3288.
[51] Sun, Y. S.; Landry, J. P.; Fei, Y. Y.; Zhu, X. D.; Luo, J. T.; Wang, X. B.; Lam, K. S. Macromolecular Scaffolds for Immobilizing Small Molecule Microarrays in Label-free Detection of Protein–Ligand Interactions on Solid Support. *Anal. Chem.* **2009**, *81*(13), 5373–5380.
[52] Sun, Y. S.; Lam, K. S.; Zhu, X. D. Determination of Bovine Serum Albumin Conjugated Drugs by Immobilization as Microarrays and Oblique-incidence Reflectivity Difference Microscopy. *Instrum. Sci. Technol.* **2014**, *42*(4), 475–485.
[53] Garrido, D.; Kim, J. H.; German, J. B.; Raybould, H. E.; Mills, D. A. Oligosaccharide Binding Proteins from *Bifidobacterium longum* subsp. *infantis Reveal a Preference for Host Glycans. PLoS One* **2011**, *6*(3), e17315.

[54] Bode, L. Recent Advances on Structure, Metabolism, and Function of Human Milk Oligosaccharides. *J. Nutr.* **2006**, *136*(8), 2127–2130.
[55] Ninonuevo, M. R.; Park, Y.; Yin, H.; Zhang, J.; Ward, R. E.; Clowers, B. H.; German, J. B.; Freeman, S. L.; Killeen, K.; Grimm, R.; Lebrilla, C. B. A Strategy for Annotating the Human Milk Glycome. *J. Agric. Food Chem.* **2006**, *54*(20), 7471–7480.
[56] Ninonuevo, M. R.; Perkins, P. D.; Francis, J.; Lamotte, L. M.; LoCascio, R. G.; Freeman, S. L.; Mills, D. A.; German, J. B.; Grimm, R.; Lebrilla, C. B. Daily Variations in Oligosaccharides of Human Milk Determined by Microfluidic Chips and Mass Spectrometry. *J. Agric. Food Chem.* **2008**, *56*(2), 618–626.
[57] Kim, J. H.; An, H. J.; Garrido, D.; German, J. B.; Lebrilla, C. B.; Mills, D. A. Proteomic Analysis of *Bifidobacterium longum* subsp. *infantis* Reveals the Metabolic Insight on Consumption of Prebiotics and Host Glycans. PLoS One **2013**, *8*(2), e57535.
[58] Thomas, P.; Nabighian, E.; Bartelt, M. C.; Fong, C. Y.; Zhu, X. D. An Oblique-incidence Optical Reflectivity Difference and LEED Study of Rare-gas Growth on a Lattice-mismatched Metal Substrate. *Appl. Phys. A* **2004**, *79*, 131–137.
[59] Zhu, X. D. Oblique-incidence Optical Reflectivity Difference from a Rough Film of Crystalline Material. *Phys. Rev. B* **2004**, *69*, 1–5.
[60] Majka, J.; Speck, C. Analysis of Protein-DNA Interactions using Surface Plasmon Resonance. *Adv. Biochem. Eng. Biotechnol.* **2007**, *104*, 13–36.
[61] Nagata, N.; Handa, H. *Real-time Analysis of Biomolecular Interactions, Applications of BIACORE*. Springer-Verlag: Tokyo, Japan, 2000.
[62] Sun, Y. S.; Zhu, X. D. Ellipsometry-based Biosensor for Label-free Detection of Biomolecular Interactions in Micro array Format. *Sensor Mater.* **2013**, *25*(9), 673–688.